

이학학사 논문
2024년 전기

Atmospheric Neutrino Oscillation Analysis in Super-Kamiokande

2024년 12월

서울대학교 자연과학대학
물리천문학부 물리학전공

2018-19174

강종휘

Atmospheric Neutrino Oscillation Analysis in Super-Kamiokande

지도교수 유종희

이 논문을 이학학사 학위논문으로 제출함 2024월 12월

서울대학교 자연과학대학
물리천문학부 물리학전공

2018-19174

강종휘

강종휘의 학사학위 논문을 인준함

2024년 12월

지도교수 유종희 (인)

심사교수 양운기 (인)

Acknowledgements

I would like to give special thanks to my advisor, Professor Jonghee Yoo, for the mentorship and the opportunity to explore the vast world of experimental neutrino research through my research internship. The experience showed me the way to further research and deeper learning. I am also grateful to Myunggi Jo for sharing his expertise in the methodology of sensitivity studies, and to Seunghyun Jung for his countless advice and guidance during the year-long research process that would eventually turn into this thesis.

Abstract

Since the discovery of neutrino oscillations, physicists have devised numerous neutrino experiments to determine the values of oscillation parameters, including mixing angles, mass-squared differences, and CP violation. Super-Kamiokande remains one of the primary experiments for studying parameters specific to atmospheric neutrinos. This thesis focuses on a sensitivity study of the neutrino oscillation parameters using Monte Carlo simulations based on the Super-Kamiokande (SK) detector configuration. Unlike analyses using experimental data, this study employs simulated atmospheric neutrino events to explore the theoretical capabilities of the SK detector setup in constraining the oscillation parameters over 328 kton-years of exposure. Key results include the rejection of the no-oscillation case in favour of the oscillation case ($\sin^2 \theta_{23} = 0.451$) with $\sqrt{\Delta\chi^2} = 1.02$ for e-like events and 51.39 for μ -like events, the up-down asymmetry of atmospheric neutrinos of e-like and μ -like events to be 1.07 and 0.78 respectively, and finally, the determination of the 1σ confidence intervals for the oscillation parameters to be:

$$\sin^2 \theta_{23} = 0.451^{+0.103}_{-0.018}, \quad \sin^2 \theta_{13} = 0.020^{+0.030}_{-0.014}, \quad \Delta m_{32,31}^2 = (2.40^{+0.213}_{-0.301}) \times 10^{-3} \text{ eV}^2.$$

Keywords: Neutrino oscillation, neutrino oscillation probability, matter effect, up-down asymmetry, neutrino mixing angle

Student Number: 2018-19174

Contents

Acknowledgements	i
Abstract	ii
List of Tables	iv
List of Figures	vi
1 Introduction	1
1.1 Neutrino Oscillation Theory	1
1.2 Matter Effect	2
1.3 Numerical Solution to the Oscillation Probability	3
1.4 Up-down Asymmetry	7
1.5 Thesis Overview	8
2 Neutrino Oscillation Probability Generator	9
3 Simulation	13
3.1 Event Generation	13
3.2 Detector Simulation	13
3.3 Event Reconstruction	13
4 Sample Selection	15
4.1 Data Reduction	15
4.2 Sample Selection	15
5 Atmospheric Neutrino Oscillation Analysis	19
5.1 Analysis Procedure	19
5.1.1 $\Delta\chi^2$ Calculation	19
5.1.2 $\pm 1\sigma$ Error Calculation	20
5.2 Atmospheric Neutrino Oscillation Results	20
6 Conclusion	24
Bibliography	26
국문초록	27

List of Tables

2.1	Specifications of the simplified PREM.	10
4.1	True vs. reconstructed vertex and direction error after each cut. FV = fiducial volume, SumQ = total charge.	16

List of Figures

1.1	Feynman diagrams of the coherent forward elastic weak CC and NC scatterings.	2
1.2	The up-down asymmetry discovered in muon neutrino data, taken from Kajita's 2016 Nobel lecture.	7
2.1	Muon-to-electron flavour oscillation probabilities of atmospheric neutrinos as a function of cosine zenith angle and neutrino energy, in the normal mass ordering scenario, taken from the 2023 Super-Kamiokande atmospheric neutrino study. The assumed oscillation parameters for the plot are $\sin^2 \theta_{23} = 0.5$, $\sin^2 \theta_{13} = 0.022$, $\sin^2 \theta_{12} = 0.307$, $ \Delta m_{32,31}^2 = 2.4 \times 10^{-3}$ eV ² , $\Delta m_{21}^2 = 7.53 \times 10^{-5}$ eV ² , and $\delta_{\text{CP}} = -\pi/2$	10
2.2	Oscillation probabilities of atmospheric neutrinos as a function of cosine zenith angle and neutrino energy, in the normal mass ordering scenario, generated using the custom oscillation probability generator. The same oscillation parameters from Figure 2.1 are used.	11
2.3	A visual representation of the simplified PREM. In the figure, atmospheric neutrino ν_A experiences 6 oscillation steps including the atmosphere, and ν_A experiences 4 oscillation steps.	11
2.4	Difference of muon-to-muon oscillation probability for PREM vs. simplified PREM.	12
3.1	Illustration of the Super-Kamiokande detector.	14
4.1	Charge distribution of simulated 30 MeV electron events.	16
4.2	Vertex (above) and direction (below) error distribution plotted for e-like (left) and μ -like (right) events. The blue (red) line indicates the error between true data and uncut (cut) data. The entire cut reduces the event rate from 88,542 to 56,844 for e-like events, and from 147,901 to 89,107 for μ -like events.	17
4.3	Reconstructed momentum vs. total charge of simulated e-like and μ -like events. The orange lines show that electrons produce significantly more photoelectrons at low energies.	18
4.4	Momentum distribution of simulated e-like and μ -like events. The orange arrow on the μ -like plot indicates a momentum threshold.	18
5.1	The zenith angle distributions of atmospheric neutrino events, corresponding to 328 kton-years of exposure in the Super-Kamiokande. The above set of histograms are references taken from the Super-Kamiokande collaboration. The dots represent data, blue represents non-oscillated Monte Carlo predictions, and red represents the best fit expectations for neutrino oscillations. The set below is the result of this experiment, using Monte Carlo simulations. Blue indicates simulation without, and red indicates simulation with oscillations.	22

- 5.2 1D $\Delta\chi^2$ profiles of the fitted oscillation parameters, θ_{23} , θ_{13} , and $\Delta m_{32,31}^2$. On the left are the references taken from the 2023 Super-Kamiokande study. Solid lines correspond to the data fit, and dashed lines correspond to the Monte Carlo expectation. Orange corresponds to inverted mass ordering, and blue corresponds to normal mass ordering. On the right are the analyses from this experiment that uses Monte Carlo simulation. The grey dotted line shows the 1σ limit. 23

Chapter 1

Introduction

1.1 Neutrino Oscillation Theory

One of the most notable properties of neutrinos is neutrino oscillation. Neutrino oscillation describes the phenomenon of neutrinos transitioning between flavour states during propagation. The cause in this behaviour lies in the misalignment of the neutrino flavour eigenstates, which dictate the interaction, with the mass eigenstates, which govern the propagation. It was first proposed as a solution to the solar and atmospheric neutrino problems, where experiments observed deficits in neutrino events compared to the expected rate.

The flavour state of a neutrino can be expressed as a superposition of the mass eigenstates:

$$|\nu_\alpha\rangle = \sum_k U_{\alpha k}^* |\nu_k\rangle, \quad (\alpha = e, \mu, \tau) \quad (1.1)$$

where $U_{\alpha k}$ are the elements of the unitary mixing matrix. To describe the time evolution of neutrinos, we solve the Schrödinger equation using the Hamiltonian of the mass eigenstate, with only the orthonormal mass states considered for simplicity:

$$H|\nu_k\rangle = E_k |\nu_k\rangle \quad (1.2)$$

$$i \frac{d}{dt} |\nu_k(t)\rangle = H |\nu_k(t)\rangle \quad (1.3)$$

The solution takes the form of a plane wave motion:

$$|\nu_k(t)\rangle = e^{-iE_k t} |\nu_k\rangle \quad (1.4)$$

Substituting this time-dependent mass state solution back into Equation 1.1, and using the unitary relation of the mixing matrix to express the mass states in terms of flavour states, we obtain an expression of the flavour states as a superposition of different flavour states:

$$|\nu_\alpha(t)\rangle = \sum_{\beta=e,\mu,\tau} \left(\sum_k U_{\alpha k}^* e^{-iE_k t} U_{\beta k} \right) |\nu_\beta\rangle \quad (1.5)$$

The transition probability from flavour state $\alpha \rightarrow \beta$ is the absolute square of the amplitude of $|\nu_\beta\rangle$:

$$P(\nu_\alpha \rightarrow \nu_\beta)(t) = |A(\nu_\alpha \rightarrow \nu_\beta)(t)|^2 = \sum_{k,j} U_{\alpha k}^* U_{\beta k} U_{\alpha j} U_{\beta j}^* e^{-i(E_k - E_j)t} \quad (1.6)$$

Because neutrinos are ultrarelativistic due to their small mass, we can approximate:

$$E_k - E_j \approx \frac{\Delta m_{kj}^2}{2E}, \quad t \approx L \quad (1.7)$$

where Δm_{kj}^2 is the squared-mass difference, and L is the source-to-detector path length. Based on these approximations, we get the expression for the neutrino oscillation probability, as a function of neutrino energy and path length:

$$P(\nu_\alpha \rightarrow \nu_\beta)(L, E) = \sum_{k,j} U_{\alpha k}^* U_{\beta k} U_{\alpha j} U_{\beta j}^* \exp\left(-i \frac{\Delta m_{kj}^2 L}{2E}\right) \quad (1.8)$$

Here, we can understand that the path length, neutrino energy, and the squared-mass differences – which are physical constants – determine the phase of neutrino oscillation, while the amplitude of the probability is purely dependent on the mixing matrix.

1.2 Matter Effect

The previous section described neutrino oscillation in vacuum. When neutrinos propagate through matter, they experience coherent forward elastic scattering with electrons and nucleons, creating an *effective potential*, which affects oscillation.

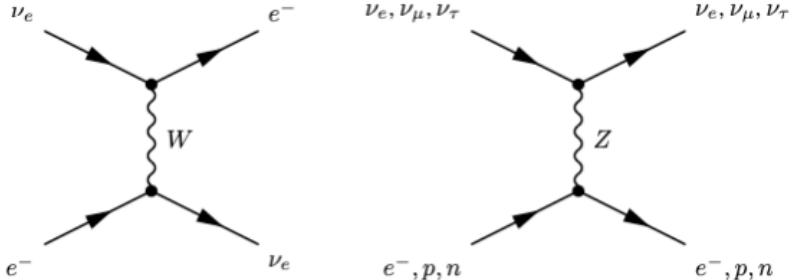


Figure 1.1: Feynman diagrams of the coherent forward elastic weak CC and NC scatterings.

The effective charged-current (CC) and neutral-current (NC) Hamiltonians are given as

$$\bar{H}_{\text{eff}}(x) = \sum_{\alpha=e,\mu,\tau} V_\alpha (\bar{\nu}_{\alpha L}(x) \gamma^0 \nu_{\alpha L}(x)), \quad (1.9)$$

$$V_\alpha = V_{\text{CC}} \delta_{\alpha e} + V_{\text{NC}} = \sqrt{2} G_F (N_e \delta_{\alpha e} - \frac{1}{2} N_n) \quad (1.10)$$

where G_F is the Fermi constant and N_e, N_n are the electron and neutron densities of the medium [1].

The effective Hamiltonian including the contribution from the matter potential is then substituted back into Equation 1.3, and the resulting Schrödinger equation is solved to derive the neutrino oscillation probability in matter.

A neutrino's probability to transition from one flavour to another can be maximised when the properties of the medium it is travelling through matches the properties of the neutrino. This is called the MSW effect. To understand how the different parameters bring about the MSW effect, we consider the simpler case of two-flavour oscillations. In this case, the transition probabilities in vacuum and matter can be simplified to:

$$\begin{aligned} P_{\text{vacuum}} &= \sin^2 2\theta \sin^2 \left(\frac{\pi L}{\lambda} \right), \\ P_{\text{matter}} &= \frac{1}{W^2} \sin^2 2\theta \sin^2 \left(\frac{\pi LW}{\lambda} \right), \end{aligned} \quad (1.11)$$

where

$$\lambda = \frac{\pi E_\nu}{1.27 \Delta m^2} \quad (1.12)$$

and

$$W^2 = \sin^2 2\theta + \left[\frac{2\sqrt{2}G_F n_e E_\nu}{\Delta m^2} - \cos 2\theta \right] \quad (1.13)$$

where n_e is the electron density, λ is a quantity defined as the oscillation length, and W^2 is a parameter that takes account for the matter effect. Note that when $W^2 = 1$, the probability in matter equals that in vacuum. However, when this parameter is minimised, with the resonance condition of

$$\frac{2\sqrt{2}G_F n_e E_\nu}{\Delta m^2} = \cos 2\theta, \quad (1.14)$$

the transition probability is maximised, causing what is called MSW resonance. This resonance condition requires

$$\sqrt{2}G_F n_e = \frac{1.2 \cos 2\theta}{\lambda} \quad (1.15)$$

which is a specific configuration of the properties of both the medium and the neutrino that travels through it.

1.3 Numerical Solution to the Oscillation Probability

Writing the neutrino oscillation probability calculation in matrix form, we begin with the statement that flavour and mass eigenstates are related by the PMNS mixing matrix:

$$\begin{pmatrix} \nu_e \\ \nu_\mu \\ \nu_\tau \end{pmatrix} = \begin{pmatrix} U_{e1} & U_{e2} & U_{e3} \\ U_{\mu 1} & U_{\mu 2} & U_{\mu 3} \\ U_{\tau 1} & U_{\tau 2} & U_{\tau 3} \end{pmatrix} \begin{pmatrix} \nu_1 \\ \nu_2 \\ \nu_3 \end{pmatrix} \quad (1.16)$$

The PMNS matrix can be represented with sines and cosines of the mixing angles as

$$U = \begin{pmatrix} 1 & 0 & 0 \\ 0 & \cos \theta_{23} & \sin \theta_{23} \\ 0 & -\sin \theta_{23} & \cos \theta_{23} \end{pmatrix} \begin{pmatrix} \cos \theta_{13} & 0 & \sin \theta_{13} e^{i\delta} \\ 0 & 1 & 0 \\ -\sin \theta_{13} e^{i\delta} & 0 & \cos \theta_{13} \end{pmatrix} \begin{pmatrix} \cos \theta_{12} & \sin \theta_{12} & 0 \\ -\sin \theta_{12} & \cos \theta_{12} & 0 \\ 0 & 0 & 1 \end{pmatrix} \quad (1.17)$$

Neutrino oscillations in vacuum are governed by the Hamiltonian

$$H_{\text{vac}} = \frac{1}{2E} U \begin{pmatrix} 0 & 0 & 0 \\ 0 & \Delta m_{21}^2 & 0 \\ 0 & 0 & \Delta m_{31}^2 \end{pmatrix} U^\dagger \quad (1.18)$$

and the oscillation probability is given as

$$P(\nu_\alpha \rightarrow \nu_\beta) = |A_{\alpha\beta}|^2, \quad A = \exp(-iHL) \quad (1.19)$$

To solve for the probability, the equations are evaluated by determining the eigenvalues and eigenvectors, and determining H :

$$A = V \begin{pmatrix} e^{-\frac{i\lambda_1 L}{2E}} & 0 & 0 \\ 0 & e^{-\frac{i\lambda_2 L}{2E}} & 0 \\ 0 & 0 & e^{-\frac{i\lambda_3 L}{2E}} \end{pmatrix} V^\dagger \quad (1.20)$$

As explained in the previous section, the calculation of oscillation probability for neutrinos travelling through matter requires an additional matter term in the Hamiltonian, coming from the matter potential. In matrix form, the effective Hamiltonian becomes

$$H = H_{\text{vac}} + \frac{1}{2E} \begin{pmatrix} a & 0 & 0 \\ 0 & 0 & 0 \\ 0 & 0 & 0 \end{pmatrix}, \quad a = 2\sqrt{2}G_F N_e E = 1.52 \times 10^{-4} \left(\frac{Y_e \rho}{g \text{ cm}^3} \right) \left(\frac{E}{\text{GeV}} \right) \text{ eV}^2 \quad (1.21)$$

In this case, diagonalising H becomes nontrivial. The algorithm for diagonalising H in vacuum is as follows:

First, the square elements of U and J , the Jarlskog invariant [2], are calculated:

$$|U_{e2}|^2 = c_{13}^2 s_{12}^2, \quad |U_{e3}|^2 = s_{13}^2, \quad |U_{\mu 3}|^2 = c_{13}^2 s_{23}^2, \quad |U_{\mu 2}|^2 = c_{12}^2 c_{23}^2 + s_{13}^2 s_{12}^2 s_{23}^2 - 2 J_{rr} \cos \delta \quad (1.22)$$

$$J = J_{rr} c_{13}^2 \sin \delta, \quad \text{with} \quad J_{rr} = \sqrt{c_{12}^2 c_{23}^2 s_{13}^2 s_{12}^2 s_{23}^2} \quad (1.23)$$

Then the appearance and disappearance probabilities are:

$$P_{\alpha\alpha} = 1 - 4 \sum_{i>j} |U_{\alpha i}|^2 |U_{\alpha j}|^2 \sin^2 \Delta_{ij} \quad (1.24)$$

$$P_{\alpha\beta} = -4 \sum_{i>j} R_{\alpha\beta}^{ij} \sin^2 \Delta_{ij} - 8 J_{\alpha\beta} \sin \Delta_{21} \sin \Delta_{31} \sin \Delta_{32} \quad (1.25)$$

$$\Delta_{ij} = \frac{\Delta m_{ij}^2 L}{4E}, \quad R_{\alpha\beta}^{ij} = R(\langle U_{\alpha i} U_{\beta j}^* U_{\alpha j}^* U_{\beta i} \rangle) = \frac{1}{2} (|U_{\alpha k}|^2 |U_{\beta k}|^2 - |U_{\alpha i}|^2 |U_{\beta i}|^2 - |U_{\alpha j}|^2 |U_{\beta j}|^2) \quad (1.26)$$

In matter, we need to replace

$$(|U_{\alpha i}|^2, J, \Delta m_{ij}^2) \rightarrow (|V_{\alpha i}|^2, J_{\text{mat}}, \Delta \lambda_{ij}) \quad (1.27)$$

by solving the characteristic equation and calculating the combinations of the elements of the eigenvectors. The problem of deriving an exact solution is computationally expensive.

For the neutrino oscillation probability generator developed for this thesis, Peter B. Denton and Stephen J. Parke's numerical solution [3] was adapted.

In their solution, the trace, determinant, and the diagonal elements of H are used to solve the characteristic equation:

$$X(\lambda) = \lambda^3 - A\lambda^2 + B\lambda - C = 0 \quad (1.28)$$

$$A = (2E)\text{Tr}[H] = \Delta m_{21}^2 + \Delta m_{31}^2 + a \quad (1.29)$$

$$B = (2E)^2 \frac{1}{2} (\text{Tr}^2[H] - \text{Tr}[H^2]) = \Delta m_{21}^2 \Delta m_{31}^2 + a (\Delta m_{21}^2 (1 - |U_{e2}|^2) + \Delta m_{31}^2 (1 - |U_{e3}|^2)) \quad (1.30)$$

$$C = (2E)^3 \text{Det}[H] = a \Delta m_{21}^2 \Delta m_{31}^2 |U_{e1}|^2 \quad (1.31)$$

Solving this characteristic equation analytically is computationally expensive. Instead, by borrowing an approximate solution by Denton, Minakata, and Parke (DMP) [4, 5],

$$\lambda_3 = \Delta m_{31}^2 + \frac{1}{2} \Delta m_{ee}^2 \left(x - 1 + \sqrt{(1-x)^2 + 4x s_{13}^2} \right) \quad (1.32)$$

$$x \equiv \frac{a}{\Delta m_{ee}^2}, \quad \Delta m_{ee}^2 \equiv \Delta m_{31}^2 - s_{12}^2 \Delta m_{21}^2 \quad (1.33)$$

Then the remaining eigenvalues can be calculated by solving

$$\lambda_1 + \lambda_2 = A - \lambda_3, \quad \lambda_1 \lambda_2 = \frac{C}{\lambda_3} \quad (1.34)$$

$$\Delta \lambda_{21} = \sqrt{(A - \lambda_3)^2 - \frac{4C}{\lambda_3}} \quad (1.35)$$

The coefficients of the Eigenvector-Eigenvalue identity are then computed using the Le Verrier-Faddeev algorithm [6]:

$$S_{\alpha\alpha} = (2E) (\text{Tr}[H]I - H)_{\alpha\alpha} = \Delta m_{21}^2 (1 - |U_{\alpha 2}|^2) + \Delta m_{31}^2 (1 - |U_{\alpha 3}|^2) + a(1 - \delta_{\alpha e}) \quad (1.36)$$

$$T_{\alpha\alpha} = (2E)^2 \text{Adj}[H]_{\alpha\alpha} = \Delta m_{21}^2 \Delta m_{31}^2 |U_{\alpha 1}|^2 + a(1 - \delta_{\alpha e}) (\Delta m_{21}^2 |U_{\beta 2}|^2 + \Delta m_{31}^2 |U_{\beta 3}|^2) \quad (1.37)$$

to obtain

$$|V_{\alpha i}|^2 = \frac{\lambda_i^2 - S_{\alpha\alpha} \lambda_i + T_{\alpha\alpha}}{\Delta \lambda_{ij} \Delta \lambda_{ik}} \quad (1.38)$$

The Jarlskog invariant in matter can be computed using the Naumov-Harrison-Scott (NHS) identity [7, 8]:

$$J_{\text{mat}} = J \prod_{i>j} \left(\frac{\Delta m_{ij}^2}{\Delta \lambda_{ij}} \right) \quad (1.39)$$

Using the replacement parameters obtained, we can calculate the oscillation probabilities in matter.

1.4 Up-down Asymmetry

Atmospheric neutrinos shower down from all directions, and because neutrinos can travel through matter, a detector near the surface of the Earth can detect atmospheric neutrinos flying from below through the Earth, called ‘up-going’ neutrinos, as well as those flying from above, called ‘down-going’ neutrinos. In 1998, atmospheric neutrino data collected in the Super-Kamiokande showed an unexpected deficit in up-going flux, compared to down-going flux; in other words, an up-down asymmetry. Up-down asymmetry is simply defined as the ratio of up-going to down-going event rate.

This discovery turned out to be a monumental leap for neutrino physics, as this phenomenon was later explained by and led to the discovery of neutrino oscillations, which require neutrinos to have nonzero mass. Up-going neutrinos travel through a longer path length through the Earth, and this, on top of the matter effect that enhances oscillation probability, results in a fraction of incoming muon neutrinos transitioning to tau neutrinos, leading to a deficit. Up-down asymmetry is prevalent in muon neutrinos, but not electron neutrinos, due to its small mixing angle, θ_{13} . The generation of atmospheric neutrino Monte Carlo simulation data and the calculation of oscillation probabilities in this thesis will allow us to observe the up-down asymmetry in muon neutrinos and recreate Takaaki Kajita’s Nobel Prize-winning discovery in 1998, as shown in Figure 1.2. [9]

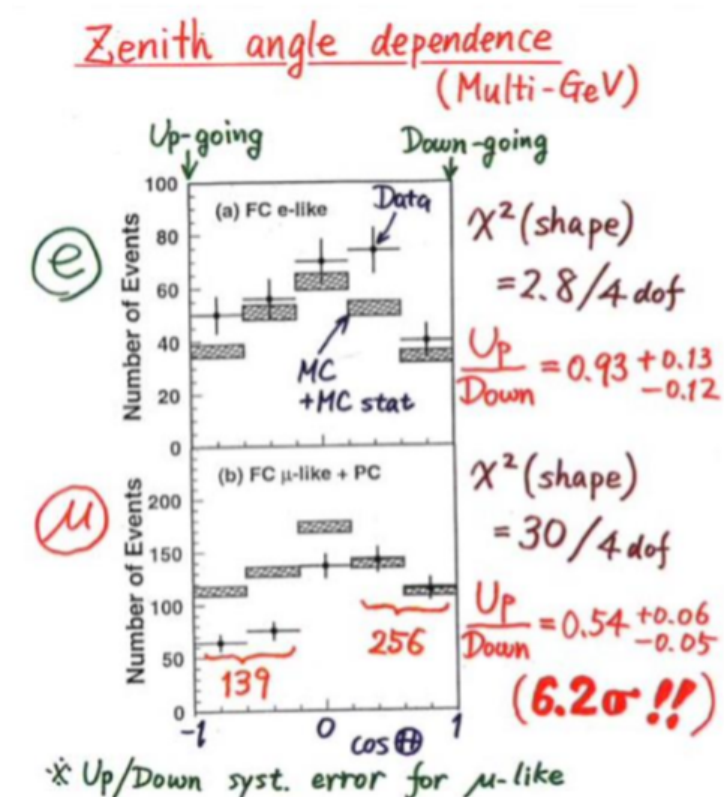


Figure 1.2: The up-down asymmetry discovered in muon neutrino data, taken from Kajita’s 2016 Nobel lecture.

1.5 Thesis Overview

This thesis will present a determination of the confidence level required to reject the no-oscillation hypothesis, as well as measurements of the $\pm 1\sigma$ confidence intervals of $\sin^2 \theta_{23}$, $\sin^2 \theta_{23}$, and $\Delta m_{32,31}^2$ around the true values. In addition, the up-down asymmetry of electron and muon neutrinos will be evaluated. The atmospheric neutrino data used is taken from a Monte Carlo simulation based of the SK configuration over 328 kton-years of exposure, overlain with a custom-developed neutrino oscillation probability generator. The development of the probability generator is described in Chapter 2, and the simulation process is described in Chapter 3. The processing of the simulated data is described in Chapter 4, and the analysis method is presented in Chapter 4, with the analysis results presented in Chapter 5.

Chapter 2

Neutrino Oscillation Probability Generator

This work aims to study the effect of neutrino oscillation and evaluate the Super-Kamiokande detector's capability to measure the oscillation parameter, θ_{23} , using only Monte Carlo simulated data. Because the simulation does not take into account neutrino oscillation, a custom oscillation probability generator was developed and applied to the simulated data.

As part of the verification method of the oscillation probability generator, and for the additional purpose of observing the matter effect resonance region, the generator was used to plot the neutrino oscillation probability as a function of cosine zenith angle and neutrino energy. Figure 2.1 shows the reference oscillation probability plot from the 2023 Super-Kamiokande atmospheric neutrino study [10]. The right diagram shows its reproduction using the custom oscillation probability generator. Figure 2.2 shows the entire set of custom-generated probability plots for all 9 oscillation modes, including the reproduction of the reference plot for muon-to-electron oscillation. It can be seen in the muon-to-electron neutrino oscillation mode that matter effect resonance occurs primarily below $\cos \theta_z = -0.5$ and between 2–10 GeV of neutrino energy.

The oscillation probability function that serves as the basis of the algorithm is derived from Denton and Parke's numerical solution, as explained in Chapter 1.3. The algorithm borrows from NuFast, which is the probability calculator algorithm based on this numerical solution [3].

In order to take into account the matter effect of atmospheric neutrinos traveling through Earth, a simplified version of the Preliminary Reference Earth Model (PREM)—which assumes the Earth as a sphere with four distinct layers, each with constant density—was implemented in conjunction with the NuFast-based probability calculator to provide density inputs for the function. Figure 2.3 shows the internal structure of a simplified PREM model, and the density and distance specifications are listed in Table 2.1 [11]. The algorithm calculates the path length for each layer as a function of the zenith angle and uses them to compute a weighted average density value to be used as a parameter in the probability function along with the total path length. This estimation method yields a highly accurate result compared to a dynamic density calculation method; however, the limitation comes from the simplification of the PREM. Figure 2.4

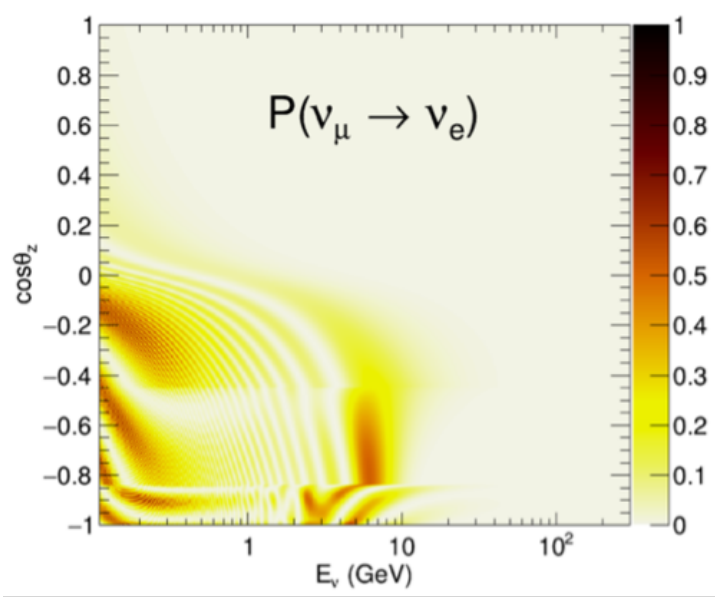


Figure 2.1: Muon-to-electron flavour oscillation probabilities of atmospheric neutrinos as a function of cosine zenith angle and neutrino energy, in the normal mass ordering scenario, taken from the 2023 Super-Kamiokande atmospheric neutrino study. The assumed oscillation parameters for the plot are $\sin^2 \theta_{23} = 0.5$, $\sin^2 \theta_{13} = 0.022$, $\sin^2 \theta_{12} = 0.307$, $|\Delta m_{32,31}^2| = 2.4 \times 10^{-3}$ eV 2 , $\Delta m_{21}^2 = 7.53 \times 10^{-5}$ eV 2 , and $\delta_{\text{CP}} = -\pi/2$.

demonstrates the limitation of using a simplified PREM compared to the actual PREM. It shows certain regions where the probability error can reach up to 15% [12]. The small difference in the $E_\nu = 2\text{--}10$ GeV, $\cos \theta_z < -0.85$ region in Figure 2.1 and the corresponding muon-to-electron oscillation mode in Figure 2.2 can be attributed to this source. Simplified PREM was used despite this limitation for the sake of algorithm efficiency because the program execution speed scales linearly with the number of layers, meaning using PREM would increase the program runtime substantially.

Region	R_{\min} (km)	R_{\max} (km)	density (g/cm3)
inner core	0	1220	13.0
outer core	1220	3480	11.3
mantle	3480	5701	5.0
crust	5701	6371	3.3

Table 2.1: Specifications of the simplified PREM.

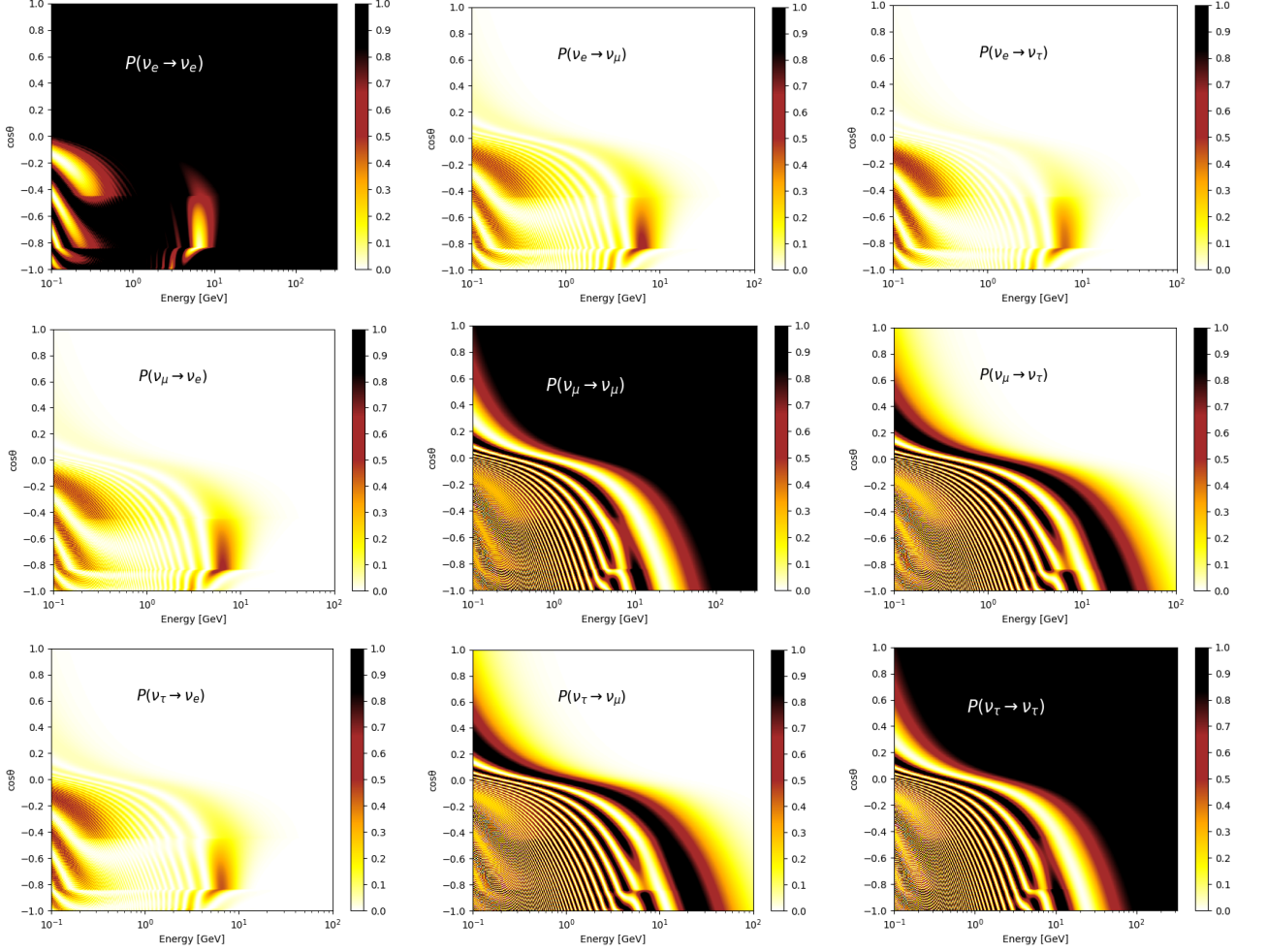


Figure 2.2: Oscillation probabilities of atmospheric neutrinos as a function of cosine zenith angle and neutrino energy, in the normal mass ordering scenario, generated using the custom oscillation probability generator. The same oscillation parameters from Figure 2.1 are used.

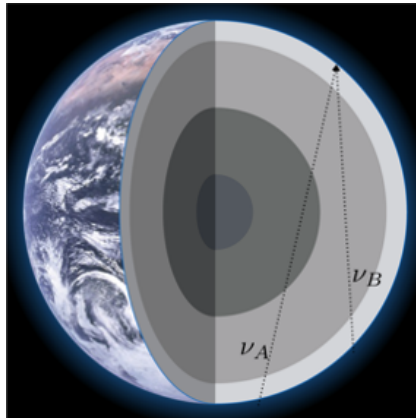


Figure 2.3: A visual representation of the simplified PREM. In the figure, atmospheric neutrino ν_A experiences 6 oscillation steps including the atmosphere, and ν_B experiences 4 oscillation steps.

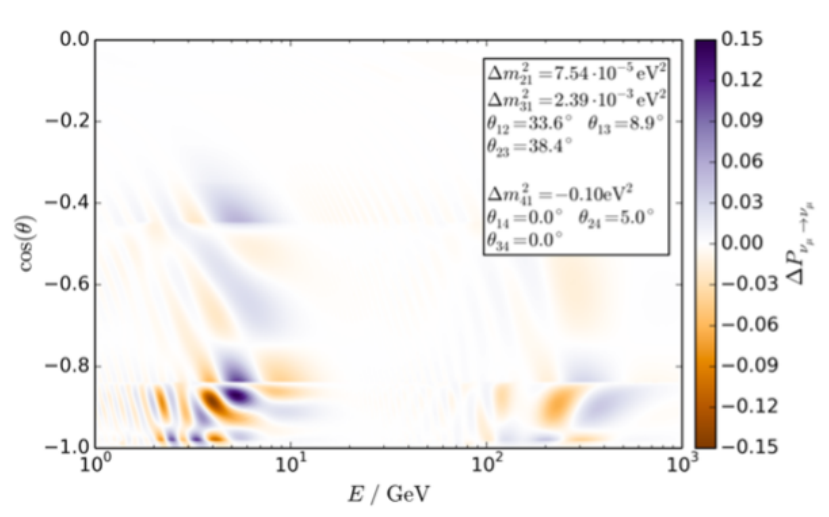


Figure 2.4: Difference of muon-to-muon oscillation probability for PREM vs. simplified PREM.

Chapter 3

Simulation

This experiment aims to understand neutrino oscillation and study the sensitivity of Super-Kamiokande purely utilising simulation data. The simulation of atmospheric neutrinos is largely a three-step process: vector generation, detector simulation, and event reconstruction.

3.1 Event Generation

Event generation is the first step of simulating atmospheric neutrinos, where neutrino flux vectors are generated using the GENIE neutrino event generator [13]. The vectors generated serve as inputs for the subsequent detector simulation and include the kinematics of primary and secondary particles from neutrino interactions. For this experiment, one million atmospheric neutrino events were generated.

3.2 Detector Simulation

The true neutrino events generated are then processed through the Geant4-based water Cherenkov detector simulation software, WCSim [14], which simulates Cherenkov radiation resulting from the particles and their subsequent detection via photomultiplier tubes (PMTs) on the detector walls. The detector geometry used is that of Super-Kamiokande [15], a 50 kt water Cherenkov detector located in Kamioka, Japan, illustrated in Figure 3.1. The simulated data mimics the detection data of a real SK experiment.

3.3 Event Reconstruction

Neutrino events are reconstructed from the detector simulation to extract meaningful physical quantities of the original particles, including particle type, momentum, interaction vertex, and direction, by analysing the Cherenkov ring patterns and PMT signals. Neutrino events are reconstructed based on the maximum likelihood method [16].

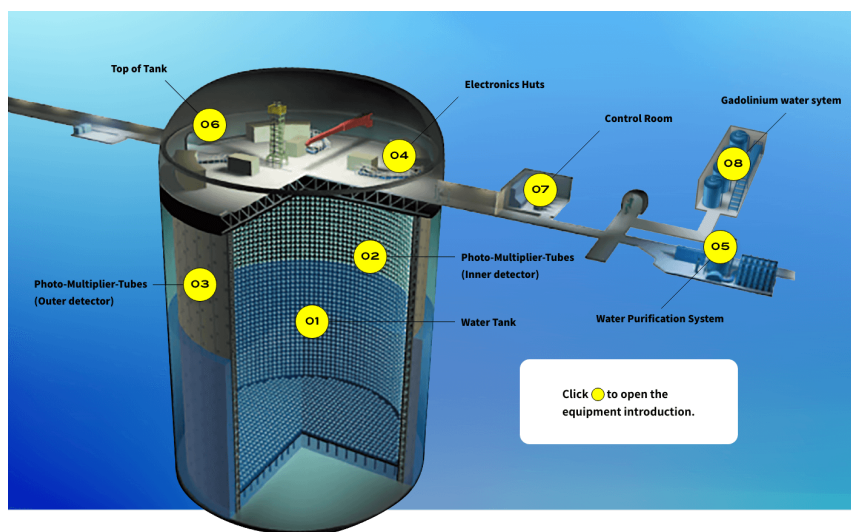


Figure 3.1: Illustration of the Super-Kamiokande detector.

Chapter 4

Sample Selection

Sample selection is a crucial first step in atmospheric neutrino oscillation analysis, as it helps identify and group events most sensitive to certain oscillation parameters while minimising systematic uncertainties and backgrounds.

4.1 Data Reduction

The two major cuts introduced in this experiment to improve data quality are for the fiducial volume and total charge detected. A significant source of background is gamma rays originating from rocks near the detector penetrating the outer detector and scattering with electrons toward the inner detector. Because these background events are scattered around the edges of the detector, a fiducial volume cut that removes events within 200 cm of the detector wall greatly enhances the data quality. A total charge cut that removes data with low charge further improves the data quality. The reference value from Thomas Wester’s atmospheric neutrino oscillation study [17] replaces this criterion with a condition of reconstructed visible energy greater than 30 MeV. Here, reconstructed visible energy, E_{vis} , refers to the sum of all momenta from reconstructed rings produced by an electron.

To convert this condition into that of the total charge, a separate simulation was run using WCSim with 500 random 30 MeV electron events. Figure 4.1 shows the charge distribution of this simulation, with a mean value of 359.9, which was rounded up to 360 photoelectrons to be used for the total charge criterion.

4.2 Sample Selection

Atmospheric neutrino candidates can largely be categorised into fully contained (FC), partially contained (PC), and upward-muon (Up- μ). For this experiment, FC samples are selected as these events occur primarily within the inner detector, where reconstruction accuracy is significantly higher. For the same reason, single-ring e-like and μ -like Sub-GeV events are selected. Single-ring e-like and μ -like events are filtered and separated by the particle identification score (PID), and

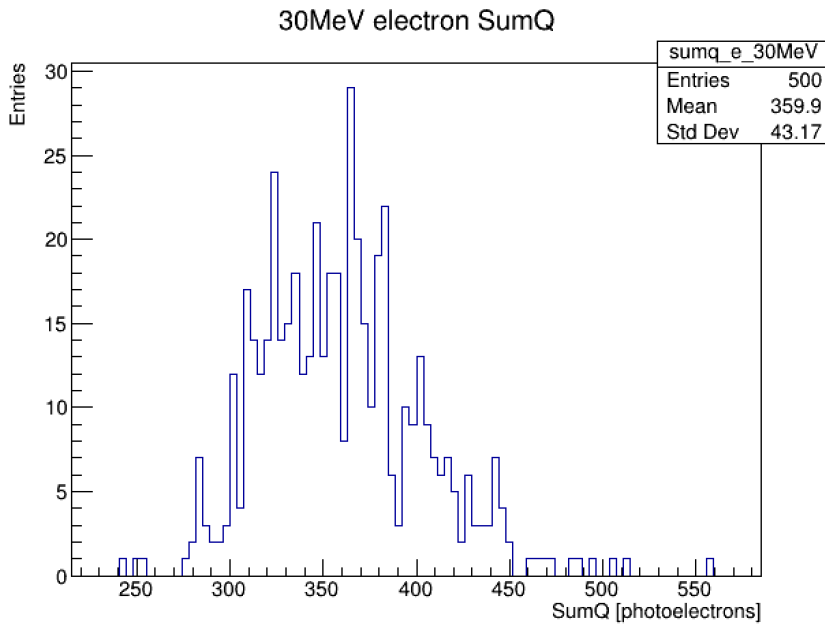


Figure 4.1: Charge distribution of simulated 30 MeV electron events.

the boundary for Sub-GeV and Multi-GeV is given as 1330 MeV.

To verify the effectiveness of the data reduction and sample selection, a set of performance tests were conducted by measuring the error between true and reconstructed data. The tests evaluate the accuracy of (a) event vertex and (b) direction, before and after the cut, as illustrated in Figure 4.2. Table 4.1 shows the vertex and direction errors after each individual cut. The errors are shown to be reduced after each cut, verifying the effectiveness of these cuts, except for the total charge cut.

Cut	Vertex error ($\mu+1\sigma$)		Direction error ($\mu+1\sigma$)	
	e-like	μ -like	e-like	μ -like
No cut	81.47	110.70	16.83	10.01
FV cut	62.90	80.89	6.10	7.78
FV + SumQ cut	62.89	77.97	6.10	6.18
FV + SumQ + Energy cut	60.77	63.17	5.69	5.74

Table 4.1: True vs. reconstructed vertex and direction error after each cut. FV = fiducial volume, SumQ = total charge.

The total charge cut primarily improves the quality of μ -like events. Since muons are approximately 200 times heavier than electrons, they require much larger momentum to surpass the same water Cherenkov threshold (speed of light in water). While low-energy electrons are still able to produce enough Cherenkov photons to be detected, low-energy muons fail to produce enough photons, and hence are removed by the total charge cut. This is evident from plotting the momentum against total charge for the simulated e-like and μ -like events, as shown in Figure 4.3. For instance, electrons with 200 MeV energy produce approximately 1800 photoelectrons, while muons with the same energy produce only up to 500 photoelectrons.

Additionally, the momentum distribution of μ -like events shows a deficiency below a certain

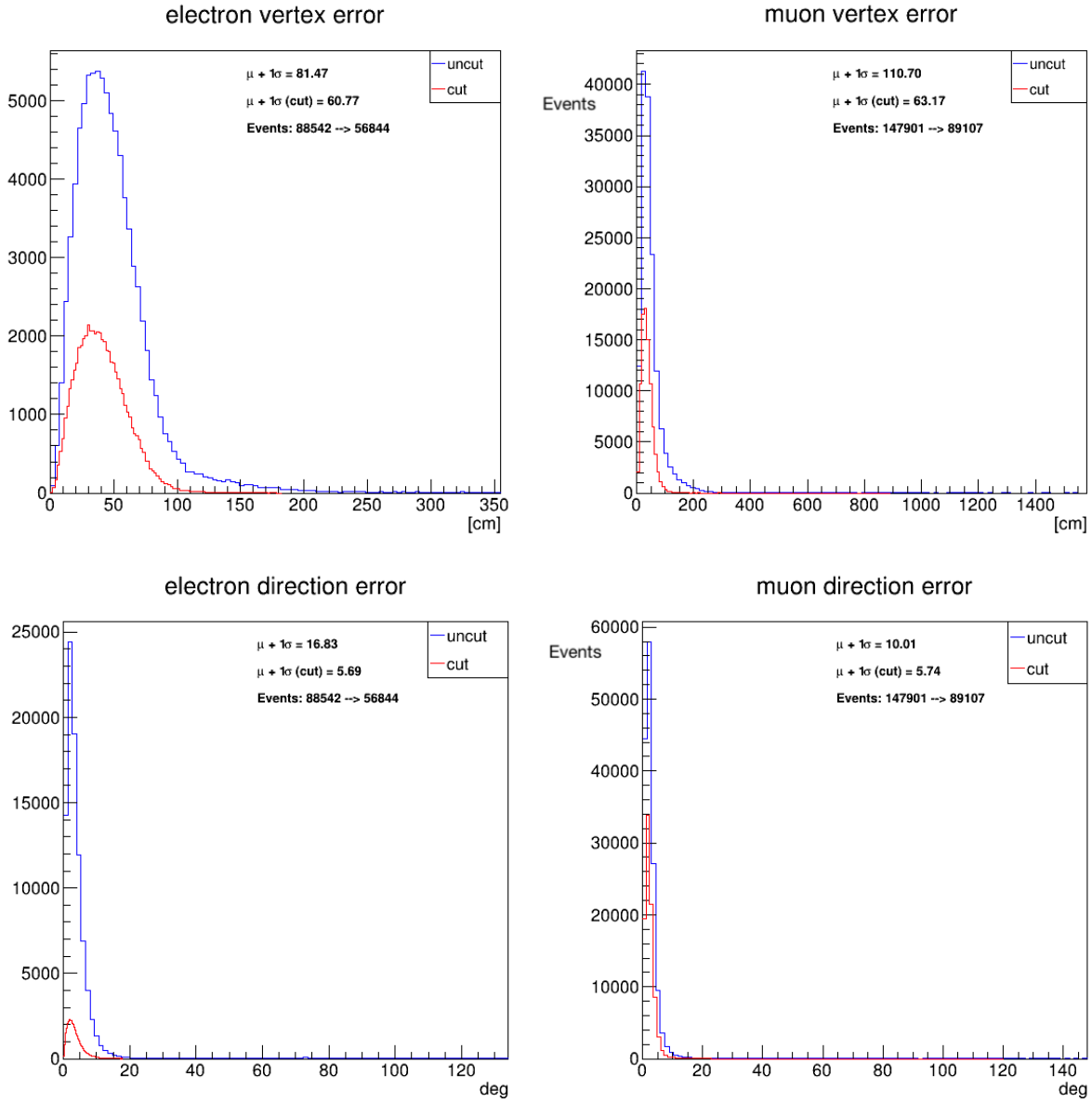


Figure 4.2: Vertex (above) and direction (below) error distribution plotted for e-like (left) and μ -like (right) events. The blue (red) line indicates the error between true data and uncut (cut) data. The entire cut reduces the event rate from 88,542 to 56,844 for e-like events, and from 147,901 to 89,107 for μ -like events.

momentum threshold, as indicated by the arrow in Figure 4.4. Events with momentum smaller than this threshold are removed by the total charge cut.

To summarise, the atmospheric neutrino sample selected for this experiment consists of FC, Sub-GeV single-ring e-like and μ -like events. Multi-GeV single-ring events are reintroduced later for part of the sensitivity study.

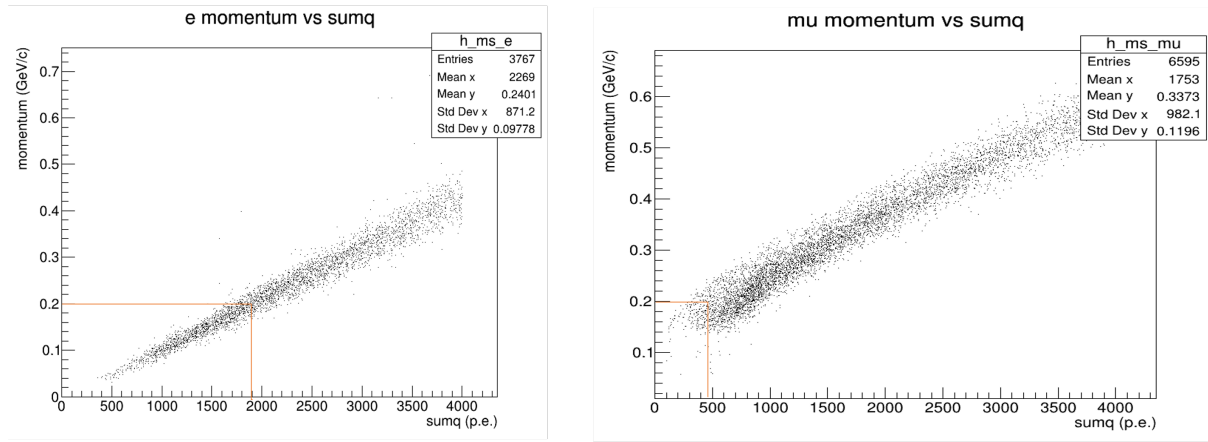


Figure 4.3: Reconstructed momentum vs. total charge of simulated e-like and μ -like events. The orange lines show that electrons produce significantly more photoelectrons at low energies.

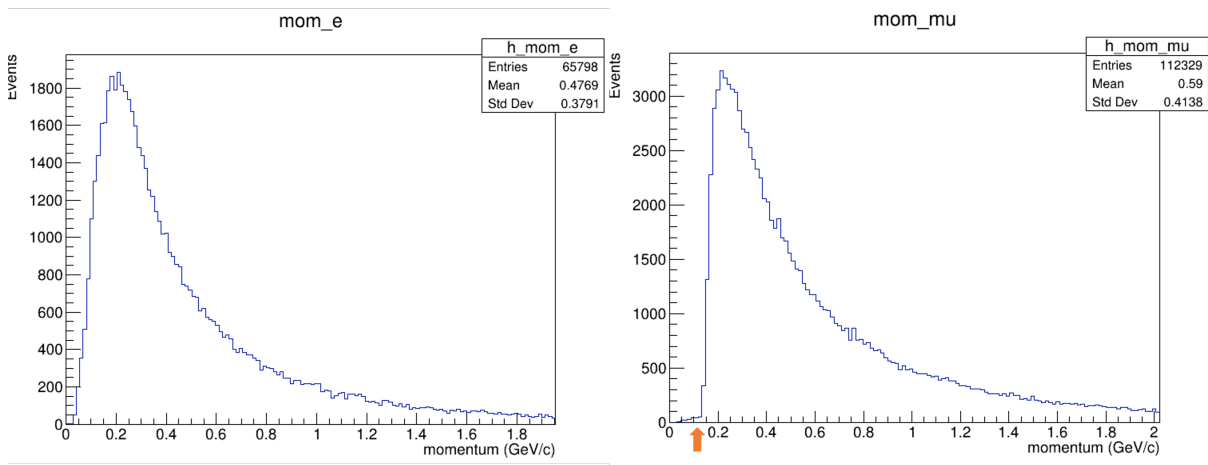


Figure 4.4: Momentum distribution of simulated e-like and μ -like events. The orange arrow on the μ -like plot indicates a momentum threshold.

Chapter 5

Atmospheric Neutrino Oscillation Analysis

5.1 Analysis Procedure

5.1.1 $\Delta\chi^2$ Calculation

The χ^2 statistic that is used to compare Monte Carlo simulations to data is calculated based on the assumption of Poisson fluctuations in the event rate for each bin. This experiment considers only the statistical uncertainty, which can be described using the Poisson likelihood function. The likelihood of observing a specific set of event counts N_{Data} in n bins, given an expected set of counts N_{MC} , can be expressed as:

$$-2 \log L = 2 \sum_{\text{bins}}^n \left(N_{\text{MC}} - N_{\text{Data}} + N_{\text{Data}} \log \frac{N_{\text{Data}}}{N_{\text{MC}}} \right) \quad (5.1)$$

The likelihood function is related to χ^2 in the following form:

$$L \propto e^{-\chi^2/2} \quad (5.2)$$

Thus, χ^2 can be expressed as:

$$\chi^2 = -2 \log L = 2 \sum_{\text{bins}}^n \left(N_{\text{MC}} - N_{\text{Data}} + N_{\text{Data}} \log \frac{N_{\text{Data}}}{N_{\text{MC}}} \right) \quad (5.3)$$

To examine the sensitivity of a detector before the collection of data, $\Delta\chi^2$ can be used as a metric to compute the difference in χ^2 values between two hypotheses, H_0 and H_1 , using Monte Carlo simulations. For this purpose, χ_0^2 and χ_1^2 are calculated for a null hypothesis and an alternative hypothesis, respectively, with the observed counts, N_{Data} , replaced with the simulated data of N_1 . Under these conditions, χ_1^2 vanishes, leaving only χ_0^2 :

$$\Delta\chi^2 = \chi_0^2 - \chi_1^2 = 2 \sum_{\text{bins}}^n \left(N_0 - N_1 + N_1 \log \frac{N_1}{N_0} \right) \quad (5.4)$$

In this experiment, we set the simulation with $\theta_{23} = 0$, which corresponds to the no-oscillation case, as the null hypothesis to reject, and the oscillation case with the current known θ_{23} value as the alternative hypothesis to accept:

$$H_0 : \sin^2 \theta_{23} = 0, \quad (5.5)$$

$$H_1 : \sin^2 \theta_{23} = 0.451 \quad (5.6)$$

[18] In order to reject the null hypothesis, the likelihood of observing the null events must be minimized. Consequently, the greater the $\Delta\chi^2$, the better we can reject the null hypothesis in favour of the alternative hypothesis. The square root of the value, $\sqrt{\Delta\chi^2}$, can be estimated to represent the confidence level to reject H_0 , according to Wilk's Theorem for large sample sizes [19].

5.1.2 $\pm 1\sigma$ Error Calculation

The second metric used for measuring the sensitivity to the oscillation parameters is the 1σ error. For this analysis, the fitting method in the 2023 Super-Kamiokande atmospheric neutrino oscillation study was used, with the exception of taking the best fit data value of $\sin \theta_{23} = 0.451$, $\sin \theta_{13} = 0.020$, and $\Delta m_{32,31}^2 = 2.40 \times 10^{-3} \text{ eV}^2$ as is. [10] The simulation's agreement with these values was evaluated using $\sqrt{\Delta\chi^2}$ at each point on a fixed grid of a number of neutrino oscillation parameter values evenly spaced between each given range, with oscillation probabilities applied to the simulated events using the oscillation parameters corresponding to each point on the grid. The grid point with the lowest $\sqrt{\Delta\chi^2}$ value is identified as the best fit of the oscillation parameter. A horizontal line is drawn at $\sqrt{\Delta\chi^2} = 1$, the 1σ limit, and the parameter values corresponding to the intercepts left and right of the minimum value are taken to be the $\pm 1\sigma$ range.

5.2 Atmospheric Neutrino Oscillation Results

The zenith angle distributions of the simulated atmospheric neutrino events from this experiment are shown in the bottom set of plots in Figure 5.1. The blue histograms show the Monte Carlo simulations with θ_{23} set to zero – essentially without oscillation, and the red histograms show those with θ_{23} set to the true value of 0.451, taken from the 2023 Super-Kamiokande study [10]. The event rate of this analysis was normalised to match the scale of the reference, which corresponds to 328 kton-years of exposure. The reference zenith angle analysis from the same study is shown in the top set of plots in Figure 5.1 for comparison. The cause of the difference

in shape between the no-oscillation μ -like MC event in the reference (top right, blue) and the equivalent part of the result (bottom right, blue) can mostly likely be attributed to the fact that the MC used in this thesis uses an open-source library, as opposed to the fortran-based library used by the SK study, and that the thesis uses the GENIE default flux information, as opposed to the atmospheric neutrino flux information used in the study. The $\sqrt{\Delta\chi^2}$ values computed from the zenith angle histograms are 1.02 for Sub-GeV e-like events and 51.39 for μ -like events.

The result from this analysis shows a significant difference in confidence levels between e-like and μ -like events. For e-like events, the null hypothesis is rejected with a confidence level of only 1σ , indicating that the Super-Kamiokande would have limited sensitivity to oscillation effects in this channel. For μ -like events, the null hypothesis is rejected at 51σ , indicating that the same detector has a much higher sensitivity to oscillation effects for muon neutrinos given 328 kton-years of exposure. This result underscores the Super-Kamiokande's ability to discern the effect of neutrino oscillations in muon neutrino events, particularly within the path length and energy scales characteristic of atmospheric neutrinos. The result is consistent with our understanding that atmospheric muon neutrinos experience greater oscillation probabilities compared to electron neutrinos due to the size difference in the mixing angles, θ_{23} and θ_{13} .

Further, the up-down asymmetry calculated from the same plots in Figure 5.1 come out to 1.07 for e-like events, and 0.78 for μ -like events. The asymmetry value in μ -like events underlines the skewness of the zenith angle distribution, as can be seen in the red histogram in the bottom right plot of Figure 5.1, and also reflects on the muon neutrino deficit that comes from up-going muon neutrinos transitioning into tau neutrinos as they travel through Earth.

The second sensitivity study method involves the minimisation of $\Delta\chi^2$. For this purpose, 1D $\Delta\chi^2$ profiles are plotted against the interested parameters of $\sin^2 \theta_{23}$, $\sin^2 \theta_{13}$, and $\Delta m_{32,31}^2$, as shown in the right side of Figure 5.2. For $\sin^2 \theta_{23}$, intercepts with the 1σ line reveal the $\pm 1\sigma$ error to be $[-0.018, +0.103]$. For $\sin^2 \theta_{13}$, the $\pm 1\sigma$ error is $[-0.014, +0.030]$, and for $\Delta m_{32,31}^2$, $[-0.301, +0.213] \times 10^{-3} \text{ eV}^2$.

While the 2023 study [10] reports error ranges of $[-0.03, +0.06]$, $[-0.011, +0.016]$, and $[-0.09, +0.07]$ for $\sin^2 \theta_{23}$, $\sin^2 \theta_{13}$, and $\Delta m_{32,31}^2$ respectively, these sets of values are taken from the data best fits, corresponding to the solid blue lines in the left of Figure 5.2. However, because this analysis was conducted using only simulated data, it would be correct to compare it to the MC expectation fits in the reference, which correspond to the blue dotted lines in the same plots. Because the error values for the MC fit are not given in the 2023 study, we can only visually estimate the intercept values, which come out as approximately $[-0.03, +0.10]$, $[-0.016, +0.032]$, and $[-0.2, +0.2]$. Considering the χ^2 statistic used in this paper does not account for systematic uncertainties, the resulting 1σ is expected to be smaller than the referenced MC error. Given this, for $\sin^2 \theta_{23}$, the negative error of -0.018 is safely within the reference range, while the positive error of 0.103 is bordered at the edge of the reference range. The errors for $\sin^2 \theta_{13}$ and $\Delta m_{32,31}^2$ are within the reference range, with the exception of the negative error for $\Delta m_{32,31}^2$. The deviations from the 2023 study most likely can be attributed to slight differences in the MC generation process and the oscillation probability calculation method as mentioned previously.

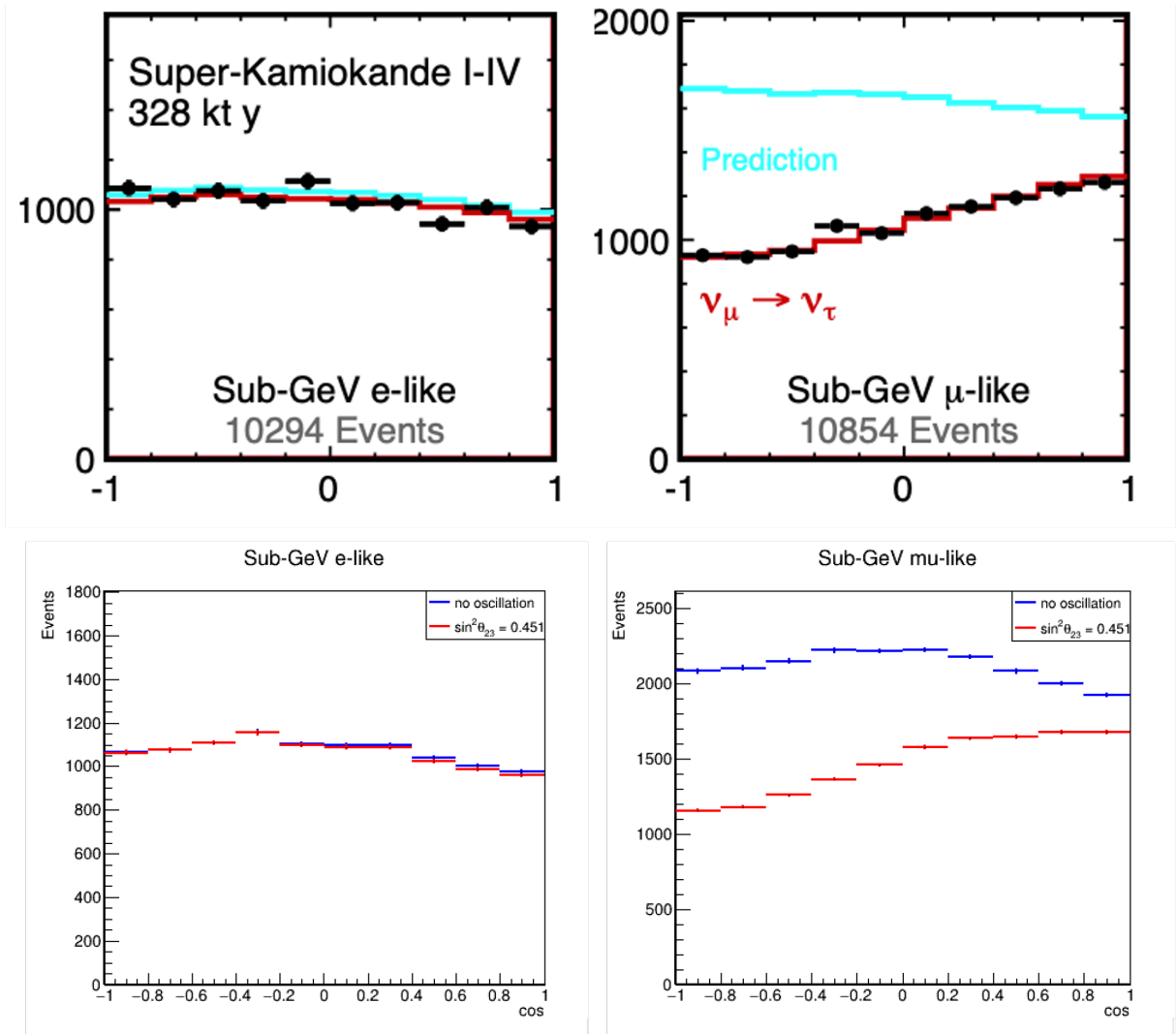


Figure 5.1: The zenith angle distributions of atmospheric neutrino events, corresponding to 328 kton-years of exposure in the Super-Kamiokande. The above set of histograms are references taken from the Super-Kamiokande collaboration. The dots represent data, blue represents non-oscillated Monte Carlo predictions, and red represents the best fit expectations for neutrino oscillations. The set below is the result of this experiment, using Monte Carlo simulations. Blue indicates simulation without, and red indicates simulation with oscillations.

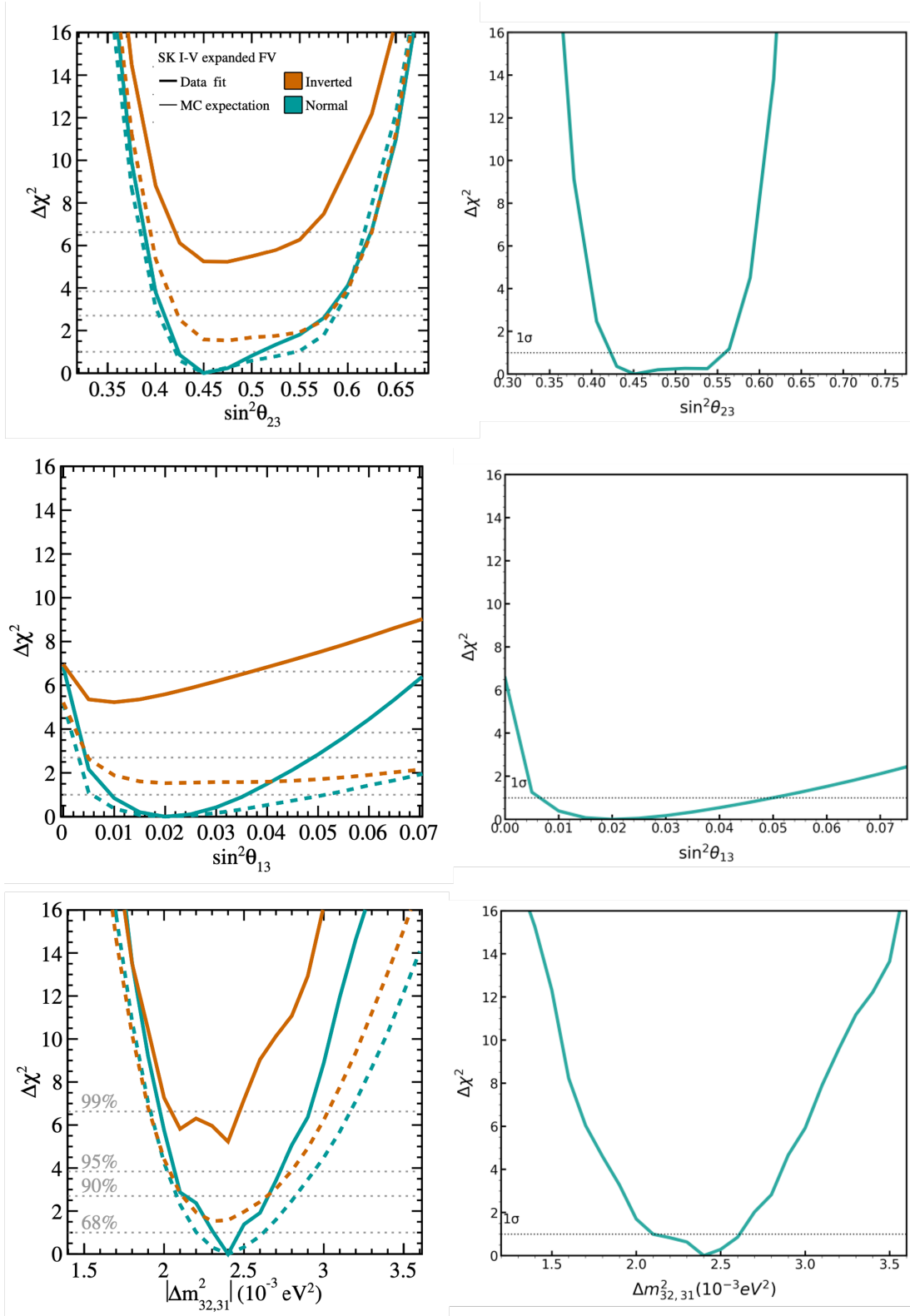


Figure 5.2: 1D $\Delta\chi^2$ profiles of the fitted oscillation parameters, θ_{23} , θ_{13} , and $\Delta m^2_{32,31}$. On the left are the references taken from the 2023 Super-Kamiokande study. Solid lines correspond to the data fit, and dashed lines correspond to the Monte Carlo expectation. Orange corresponds to inverted mass ordering, and blue corresponds to normal mass ordering. On the right are the analyses from this experiment that uses Monte Carlo simulation. The grey dotted line shows the 1σ limit.

Chapter 6

Conclusion

The parameters of oscillation, including the mixing angles and the squared-mass differences help our understanding of neutrino oscillations, as they governs the flavour transitions observed in atmospheric neutrinos. Their precise determination helps refine the oscillation model and reduces uncertainties in related parameters. This thesis focused on a sensitivity study of θ_{23} , θ_{13} , and $\Delta m_{32,31}^2$ using Monte Carlo simulations based on Super-Kamiokande detector configurations. Rather than analysing experimental data, this work explored the theoretical capabilities of the detector setup to constrain these parameters through simulated atmospheric neutrino events.

It began with developing a neutrino oscillation probability generator from scratch, based on an efficient numerical solution to the three-flavour oscillation problem. Non-oscillated neutrino events simulated through Monte Carlo generation were processed via data reduction and sample selection, before applying oscillation probabilities to it using the custom generator. Then, this set of data was analysed by studying the Super-Kamiokande's sensitivity to neutrino oscillation itself, and to the oscillation parameters via the determination of $\Delta\chi^2$ and the 1σ error. Additionally, this study investigated the up-down asymmetry in atmospheric neutrinos, a key observable arising from neutrino oscillations over varying path lengths through the Earth.

While the sensitivity study of the Super-Kamiokande provides insight into the capability of the detector in probing fundamental neutrino properties, the detector is already a well-established facility for oscillation studies, being the largest operating water Cherenkov neutrino detector in the world. Beyond evaluating the capabilities of this specific detector, this study serves as a means to deepen the understanding of neutrino oscillation and the processes involved in neutrino experiments. This work helped build experience in simulation-based neutrino studies and analysis techniques, which may be used for future studies with next-generation detectors such as Hyper-Kamiokande and KNO, in evaluating how these can further advance our understanding of fundamental neutrino properties.

Bibliography

- [1] Carlo Giunti and Chung W. Kim. *Fundamentals of Neutrino Physics and Astrophysics*. Oxford University Press, 2007.
- [2] C. Jarlskog. Commutator of the quark mass matrices in the standard electroweak model and a measure of maximal CP nonconservation. *Phys. Rev. Lett.*, 55:1039–1042, Sep 1985.
- [3] Peter B. Denton and Stephen J. Parke. Fast and accurate algorithm for calculating long-baseline neutrino oscillation probabilities with matter effects. *Physical Review D*, 110(7), October 2024.
- [4] Hisakazu Minakata and Stephen J. Parke. Simple and compact expressions for neutrino oscillation probabilities in matter. *Journal of High Energy Physics*, 2016(1), January 2016.
- [5] Peter B. Denton, Hisakazu Minakata, and Stephen J. Parke. Compact perturbative expressions for neutrino oscillations in matter. *Journal of High Energy Physics*, 2016(6), June 2016.
- [6] Asli Abdullahi and Stephen J. Parke. Neutrino oscillations in matter using the adjugate of the hamiltonian, 2023.
- [7] V.A. Naumov. Three-neutrino oscillations in matter, cp-violation and topological phases. *International Journal of Modern Physics D*, 01(02):379–399, 1992.
- [8] P.F. Harrison and W.G. Scott. Neutrino matter effect invariants and the observables of neutrino oscillations. *Physics Letters B*, 535(1–4):229–235, May 2002.
- [9] Takaaki Kajita. Nobel lecture: Discovery of atmospheric neutrino oscillations. *Rev. Mod. Phys.*, 88:030501, Jul 2016.
- [10] T. Wester, K. Abe, C. Bronner, Y. Hayato, and K. et al. Hiraide. Atmospheric neutrino oscillation analysis with neutron tagging and an expanded fiducial volume in super-kamiokande i–v. *Physical Review D*, 109(7), April 2024.
- [11] K. Abe, C. Bronner, Y. Haga, Y. Hayato, and M. et al. Ikeda. Atmospheric neutrino oscillation analysis with external constraints in super-kamiokande i–iv. *Physical Review D*, 97(7), April 2018.

- [12] Marius Wallraff and Christopher Wiebusch. Calculation of oscillation probabilities of atmospheric neutrinos using nucraft. *Computer Physics Communications*, 197:185–189, December 2015.
- [13] C. Andreopoulos, A. Bell, D. Bhattacharya, F. Cavanna, J. Dobson, and S. et al. Dytman. The genie neutrino monte carlo generator. *Nuclear Instruments and Methods in Physics Research Section A: Accelerators, Spectrometers, Detectors and Associated Equipment*, 614(1):87–104, February 2010.
- [14] WCSim. Wcsim. <https://github.com/WCSim/WCSim>, 2024.
- [15] S. Fukuda, Y. Fukuda, T. Hayakawa, E. Ichihara, and M. et al. Ishitsuka. The super-kamiokande detector. *Nuclear Instruments and Methods in Physics Research Section A: Accelerators, Spectrometers, Detectors and Associated Equipment*, 501(2–3):418–462, 2003.
- [16] M Jiang, K Abe, C Bronner, Y Hayato, and M. et al. Ikeda. Atmospheric neutrino oscillation analysis with improved event reconstruction in super-kamiokande iv. *Progress of Theoretical and Experimental Physics*, 2019(5), May 2019.
- [17] Thomas Wester. *Discerning the Neutrino Mass Ordering using Atmospheric Neutrinos in Super-Kamiokande I-V*. PhD thesis, Boston University, Boston U., 2023.
- [18] Particle Data Group. Neutrino mixing. *Review of Particle Physics, Progress of Theoretical and Experimental Physics*, 2023. Accessed: November 27, 2024.
- [19] S. S. Wilks. The large-sample distribution of the likelihood ratio for testing composite hypotheses. *The Annals of Mathematical Statistics*, 9(1):60–62, 1938. Accessed: November 27, 2024.

국문초록

중성미자 진동의 발견 이후, 섞임각, squared-mass difference, CP violation 등의 진동 매개변수 측정을 위해 여러가지 실험이 고안되어왔다. 그 중 Super-Kamiokande(SK)는 대기중성미자의 성질을 연구하는 주요 실험 중 하나이다. 본 논문에서는 SK 검출기를 기반으로한 MC 시뮬레이션을 사용하여 다양한 진동 매개변수에 대한 sensitivity 연구를 진행한다. 검출기 데이터를 분석하는 연구와 달리, 본 연구는 대기중성미자의 검출을 시뮬레이션으로 예측하고, 그 데이터를 분석함으로서 328 kton-years의 SK 검출기의 진동 매개변수 분석 능력을 측정한다. 주요 결과는 다음과 같다. 대립가설($\sin^2 \theta_{23} = 0.451$)을 이용해 중성미자 진동이 일어나지 않는다는 귀무가설을 기각하는 감도의 경우, e-like event에서 $\sqrt{\Delta\chi^2} = 1.02$, μ -like event에서 $\sqrt{\Delta\chi^2} = 51.39$ 의 결과를 얻었다. 또한 대기중성미자의 상하 비태칭의 경우 e-like 와 μ -like event에서 각각 1.07, 0.78로 계산되었다. 마지막으로 진동매개변수의 오차는 다음과 같이 추산되었다:

$$\sin^2 \theta_{23} = 0.451^{+0.103}_{-0.018}, \quad \sin^2 \theta_{13} = 0.020^{+0.030}_{-0.014}, \quad \Delta m_{32,31}^2 = (2.40^{+0.213}_{-0.301}) \times 10^{-3} \text{ eV}^2.$$

주요어: 중성미자 진동, 막깔 진동 확률, 물질 효과, 상하 비대칭, 중성미자 섞임각

학 번: 2018-19174